Charge collection in the Silicon Drift Detectors of the ALICE experiment

2010 JINST 5 P02008

(http://iopscience.iop.org/1748-0221/5/02/P02008)

PUBLISHED BY IOP PUBLISHING FOR SISSA

RECEIVED: *January 13, 2010*
ACCEPTED: *January 28, 2010*
PUBLISHED: *February 24, 2010*

Charge collection in the Silicon Drift Detectors of the ALICE experiment

B. Alessandro,[a] R. Bala,[b] G. Batigne,[a,1] S. Beolé,[b] E. Biolcati,[b,2] P. Cerello,[a] S. Coli,[a] Y. Corrales Morales,[c,a] E. Crescio,[a] P. De Remigis,[a] D. Falchieri,[d] G. Giraudo,[a] P. Giubellino,[a] R. Lea,[b] A. Marzari Chiesa,[b] M. Masera,[b] G. Mazza,[a] G. Ortona,[b] F. Prino,[a] L. Ramello,[e] A. Rashevsky,[f] L. Riccati,[a] A. Rivetti,[a] S. Senyukov,[e] M. Siciliano,[b] M. Sitta,[e] M. Subieta,[b] L. Toscano[a] and F. Tosello[a]

[a] *Istituto Nazionale di Fisica Nucleare - Sezione di Torino, Torino, Italy*
[b] *Dipartimento di Fisica Sperimentale dell'Università di Torino and INFN, Torino, Italy*
[c] *Instituto Superior de Tecnologìas y Ciencias Aplicadas (InSTEC), Havana, Cuba*
[d] *Dipartimento di Fisica dell'Università di Bologna & INFN Bologna, Bologna, Italy*
[e] *Dipartimento di Scienze e Tecnologie Avanzate dell'Università del Piemonte Orientale e Gruppo Collegato INFN, Alessandria, Italy*
[f] *Istituto Nazionale di Fisica Nucleare - Sezione di Trieste, Trieste, Italy*

E-mail: biolcati@to.infn.it

ABSTRACT: A detailed study of charge collection efficiency has been performed on the Silicon Drift Detectors (SDD) of the ALICE experiment. Three different methods to study the collected charge as a function of the drift time have been implemented. The first approach consists in measuring the charge at different injection distances moving an infrared laser by means of micrometric step motors. The second method is based on the measurement of the charge injected by the laser at fixed drift distance and varying the drift field, thus changing the drift time. In the last method, the measurement of the charge deposited by atmospheric muons is used to study the charge collection efficiency as a function of the drift time. The three methods gave consistent results and indicated that no charge loss during the drift is observed for the sensor types used in 99% of the SDD modules mounted on the ALICE Inner Tracking System. The atmospheric muons have also been used to test the effect of the zero-suppression applied to reduce the data size by erasing the counts in

[1] Now at SUBATECH, Ecole des Mines de Nantes, Université de Nantes, CNRS/IN2P3, Nantes, France.
[2] Corresponding author.

doi:10.1088/1748-0221/5/02/P02008

2010 JINST 5 P02008

cells not passing the thresholds for noise removal. As expected, the zero suppression introduces a dependence of the reconstructed charge as a function of drift time because it cuts the signal in the tails of the electron clouds enlarged by diffusion effects. These measurements allowed also to validate the correction for this effect extracted from detailed Monte Carlo simulations of the detector response and applied in the offline data reconstruction.

KEYWORDS: Particle tracking detectors; dE/dx detectors

ARXIV EPRINT: 1001.2276v1

2010 JINST 5 P02008

Contents

2010 JINST 5 P02008

1 Introduction

Large area Silicon Drift Detectors (SDDs) [1–3] equip the two intermediate layers of the Inner Tracking System (ITS) of the ALICE experiment at the LHC [4, 5]. They have been selected due to their good spatial resolution, capability of unambiguous two-dimensional position determination and possibility to provide the energy-loss measurement needed for particle identification. The operating principle of SDDs is based on the drift towards collecting anodes of the electrons produced in the sensitive volume by an ionizing particle. The transport of electrons in a direction parallel to the surface of the detector and along distances of several centimeters is achieved by creating a drift channel in the middle of the depleted bulk of a Silicon wafer, as shown in figure 1(a). Thus, the distance of the crossing point from the anodes is determined by the measurement of the drift time, as long as the drift velocity is know, which is proportional to the applied electric field E and to the electron mobility μ_e ($v = \mu_e E$). The second coordinate is obtained from the centroid of the charge distribution along the anodes.

To reach the required spatial resolution of $\approx$30 μm, either an excellent uniformity of the drift field over all the sensitive region of the detector, or to correct for the systematic errors caused by its non-uniformity is necessary, as discussed in [6]. Furthermore, the drift velocity must be known with a precision better than 0.1% in every point of the SDD sensors. This is a challenging requirement because the mobility depends on the temperature as $\mu_e \propto T(K)^{-2.4}$, so the drift speed, which is about 6.5 μm/ns at the bias voltage of 1.8 kV, varies by about 0.8%/K at room temperature.

In order to perform the study of the collection charge efficiency in the SDD, a test station has been set-up at the INFN Technological Laboratory in Turin. In the following sub-sections an overview of the ALICE SDDs and the explanation of the methods used for the data analysis will be presented. In section 2 the results obtained by using the infrared laser with two different data taking

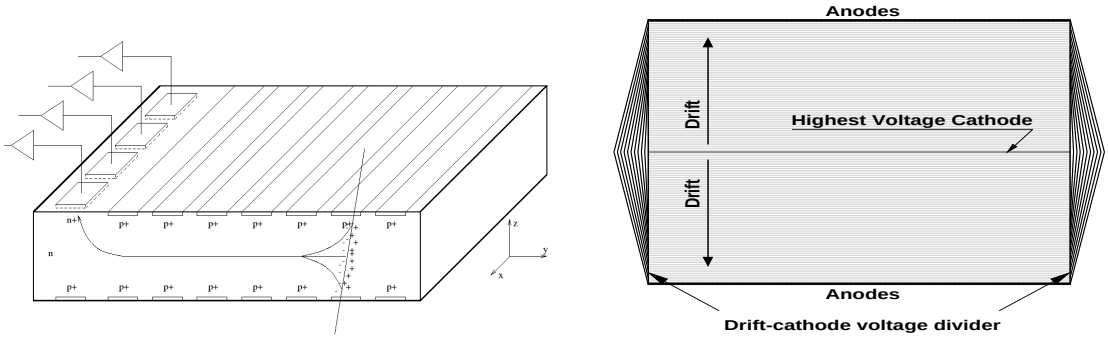

(a) (b)

Figure 1. (a) SDD operation scheme. (b) SDD module.

procedures will be reported. In section 3 the study performed with cosmic data will be presented and the results will be discussed. The conclusions of this work are addressed in the last section (section 4).

1.1 The ALICE Silicon Drift Detector

The sensor. The SDD sensors [7] of the ALICE experiment are built on n-type high-resistivity 300 μm-thick Neutron-Transmutation-Doped silicon. The active area of 7.02 $\times$ 7.53 cm^2 is split into two drift regions ($\approx$ 35 mm long) by a central cathode strip which is biased at a maximum voltage (HV) of -1700 $\div$ -2400 V. In each drift region, on both the detector surfaces, 291 p$^+$ cathode strips with 120 μm pitch are implanted as sketched in figure 1(b). A built-in voltage divider, made of Polysilicon implants, biases these cathodes at a gradually decreasing voltage from the HV applied to the central cathode down to a medium voltage (MV$\approx$ -40 V) applied to the last cathodes before the anodes. This MV is used to polarize the so-called collection region, as described in [6]. In this way, a drift field parallel to the wafer surface is generated, giving rise to a bi-directional structure: the electrons drift from the central cathode towards the anodes. The drift field $E_{\rm drift}$ is given by the ratio between the inter-cathode voltage drop $V_{\rm gap} = (HV - MV)/291$ and the cathode pitch (= 120 μm); typical operation values for $V_{\rm gap}$ are between 5.5 and 8 V, corresponding to $E_{\rm drift}$ in the 458-667 V/cm range. At the end of each of the two drift regions, the electrons produced by the crossing particle are conveyed by means of pull-up cathodes, placed below the anodes, towards an array of 256 collection anodes (294 μm pitch) connected via micro-cables to the front-end electronics. For a detailed description of the SDD sensor, see [5–7].

Front-end electronics and zero-suppression. The front-end electronics of the SDD is based on three application-specific integrated circuits (ASICs). The first one, called PASCAL, is a mixed-mode chip with 64 channels [8]. In each channel the signal coming from one anode is amplified by a charge sensitive amplifier and sampled at 40 MHz[1] by an analogue memory with 256 cells. When a trigger signal is issued, the content of the memory is frozen and the samples are digitized by a 10-bit successive-approximation ADC. One converter serves two adjacent channels, so 32 ADCs

[1] A sampling frequency of 20 MHz can also be used in order to reduce the dead time.

2010 JINST 5 P02008

are embedded on the chip. After the digitization, the data are transferred to the second stage, handled by a AMBRA chip [9]. This ASIC performs the pedestal equalization on a channel by channel basis and applies a 10 to 8 bits compression algorithm before storing the data in one of its four event buffers. Four PASCAL-AMBRA pairs are mounted on the front-end hybrid [8], which is a flex circuit made of Aluminum-Kapton cables laid-out on a carbon fiber support. Two front-end hybrids are hence necessary to read-out a full sensor. A short cable ($\approx$2 cm) connects the SDD anodes to the PASCAL inputs, while a longer one (up to 40 cm) allows the communication between the hybrids and the rest of the system and distributes the supply voltages. All the interconnections exploit the Aluminum on Kapton technology.

Two front-end hybrids are connected to the same data compression board which hosts one CARLOS chip [10]. The use of four event buffers on AMBRA allows the derandomization of the triggers, so the data transmission speed from the front-end hybrid can be tuned to the average event rate. CARLOS performs the zero suppression before sending the data via optical fiber to the so called CARLOSrx board [11]. Due to the diffusion occurring in the sensor the signals present significant tails, so the use of a simple zero suppression is problematic. A bi-dimensional compression algorithm based on a dual threshold has therefore been preferred [12]. To be accepted as a valid signal, a sample must exceed the higher threshold and have at least one neighbor above the lower one or viceversa. This allows to suppress noise spikes (isolated samples above threshold) and to preserve as much as possible the samples in the tail of the signals. Despite their amplitude these can in fact contribute significantly to the final spatial resolution because of their bigger lever arm in the centroid calculation. Moreover, a cut of these tails also affects the measurement of the deposited energy.

Charge collection. The SDDs inside the ALICE ITS have two main tasks: the first is to ensure an adequate space resolution on the particle crossing point together with good multi-track capability, while the second is to measure the specific ionization energy loss (dE/dx). Hence, the Charge Collection Efficiency (CCE) is an important characteristic of the detector quality in order to achieve the required precision in dE/dx measurements. The CCE must also be known as a function of the drift time (i.e. the time necessary for charge carriers electrons or holes, created by ionizing particles in active volume, to reach a signal readout electrode). In the SDD, the drift time can be as long as 6 microseconds. The possible reasons of a decrease in CCE are described in the following points.

1. The drifting charge carriers (electrons in the SDD case) undergo diffusion, giving rise to an electron cloud with Gaussian-like profile, both along the drift and anodes axes, with a sigma given by

$$\sigma^2 = 2Dt_{\text{drift}} + \sigma^2_{\text{time0}} \tag{1.1}$$

   where D is the diffusion coefficient: $D = K_{\text{B}}T\mu_{\text{e}}/q$, with K_{B} the Boltzmann constant, T the absolute temperature, μ_{e} the electron mobility and q the electron charge. For the ALICE Silicon Drift Detectors, $D \approx 3 \div 5\,\mu\text{m}^2/\text{ns}$.

   The electron cloud generated far from the anodes can extend up to 4 anodes in the anode direction and can last up to 200 ns along the drift direction. It may well happen that a fraction of the charge in the tails of the electron cloud does not contribute to the total collected charge,

2010 JINST 5 P02008

because it gets suppressed by the zero-suppression algorithm, described in the previous section. This fraction increases with the Gaussian width σ and consequently with increasing drift time. The zero-suppression may also affect the fraction of collected charge in case of inclined tracks which give rise to elongated clusters with a larger fraction of anode/time bin cells with signal below the thresholds. This effect is however not present in these studies because particles orthogonal to the detector surface have been used in both the laser and cosmic studies.

2. A localized defect in one of the voltage dividers could result in the voltage unbalance between corresponding drift cathodes placed on opposite SDD surfaces (see figure 1(b)). This effect leads to a shift of the bottom of the potential gutter, along which the electrons drift towards the surface where the charge can be trapped. As a consequence, it is expected to have a *step like* CCE fall-down above a given drift distance.

3. Impurities present in the depleted silicon bulk of the SDD could trap drifting charge carriers which causes a dependence of the collected charge on the carriers drift time. It is worthwhile to note that the effect of the zero-suppression algorithm mentioned in comma 1) easily fakes charge trapping.

1.2 Experimental setup and analysis methods

The test setup exploits an infrared laser and micro-metric step motors to provide the capability of generating signals in known positions in the detector. For a detailed description, see [6]. The aim of this work is to study the dependence of the collected charge on the drift time, so as to test the possible presence of systematic effects on the CCE. The studies have been performed on three Silicon Drift Detectors that were not mounted on the ALICE ITS, because they present a large number of bad channels (noisy or non-functional), but they can be used for this analysis that is performed on few selected anodes. Two modules (called A and B) have been obtained from the final production of sensor using Silicon wafers with a uniform dopant concentration. One of these (B) has a localized defect in the internal voltage divider. The third module (called C) was a prototype built from a different Silicon wafer and presents significant doping inhomogeneities [6].

Three different analysis methods have been implemented: two of them make use of the 980 nm infrared laser to generate the signal, while the third method is based on the ionization produced in the SDD sensor by atmospheric muons.

1. *Fine position scanning* consists in measuring the collected charge as a function of the drift distance (i.e. the drift time), moving the laser on a linear trajectory along the drift coordinate at fixed anode coordinate by means of micro-metric step motors.

2. *Fixed position* is based on the measurement of the collected charge when firing the laser in a fixed point (i.e. at fixed drift distance) and varying the drift field, thus changing the drift time only.

3. *Cosmic rays* is based on the measurement of the charge deposited by atmospheric muons as a function of drift time.

2010 JINST 5 P02008

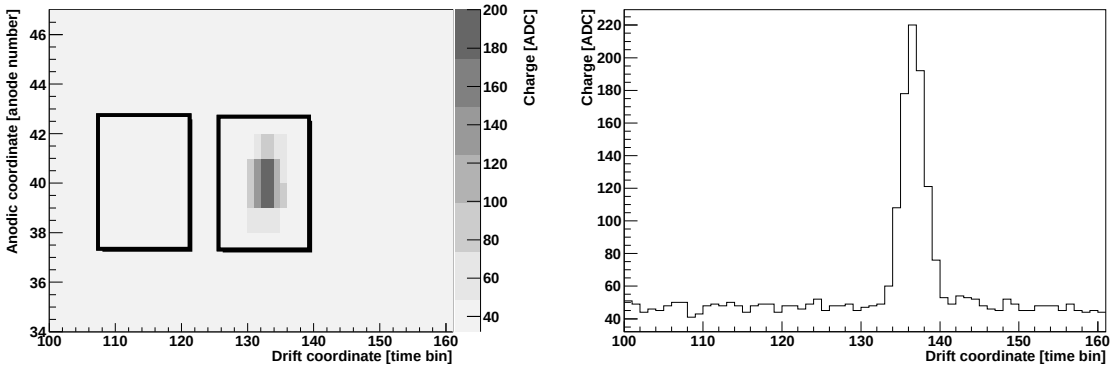

(a) (b)

Figure 2. (a) Cluster generated by a laser shot. The total charge value is obtained by subtraction of charge contained in the two rectangles. (b) Slice plot along $x-$axis: charge collected by the anode corresponding to the signal peak as a function of the drift time.

Data have been collected without enabling the zero-suppression algorithm to isolate possible effects of charge trapping and voltage divider defects. In figure 2(a) an example of a cluster produced by a laser shot in the middle between anodes 39 and 40 is shown. On the $x-$axis the drift time measured in time bins (1 time bin = 25 ns) is reported, while on the $y-$axis the anodic coordinate, defined by the anode number, is shown. The collected charge, expressed in ADC counts, is represented in gray scale. The two rectangles represent the *signal* and the *baseline* regions which are used in this analysis to extract the collected charge, as it will be explained later in this section. The plot shows 60 time bins $\times$ 17 anodes (out of 256 $\times$ 256 cells of one hybrid) where the signal *cluster* is visible. The cluster is 6 time bins $\times$ 4 anodes size, with a peak value of $\approx$ 200 ADC. The size of the cluster is not due to the size of the laser spot (which is $\approx 5 \div 10$ μm, but to charge diffusion effects. In the remaining part of the sensor an average value of $\approx$ 40 ADC is measured for the baseline. In figure 2(b) the charge collected by the anode corresponding to the signal peak is shown as a function of the drift coordinate. For this module, the average noise value (i.e. the fluctuation around the baseline) is $\approx$2.3 ADC counts. The peak signal-to-*noise* ratio, obtained after the baseline subtraction, is about 95.

A possible method to measure the total cluster charge would be to set a threshold equal to the baseline increased by few times the noise, and sum the ADC counts of the cells passing this threshold (somewhat equivalent to a zero-suppression algorithm). Anyway, with such on approach, the tails of the cluster would be cut thus affecting the measurement of the charge especially in the cases of large drift times.

Therefore a different method has been developed. The total charge of the cluster is obtained by summing the ADC counts of all the cells inside a rectangular region centered on the signal peak and sized so as to contain the entire cluster, also for the cases with maximal diffusion (i.e. largest drift time). The sum of the ADC counts in a rectangle with the same area and shifted along the drift direction is subtracted to remove the contribution of the baseline under the peak. A sketch of the two regions, called *signal rectangle* and *baseline rectangle*, is shown in figure 2(a).

2010 JINST 5 P02008

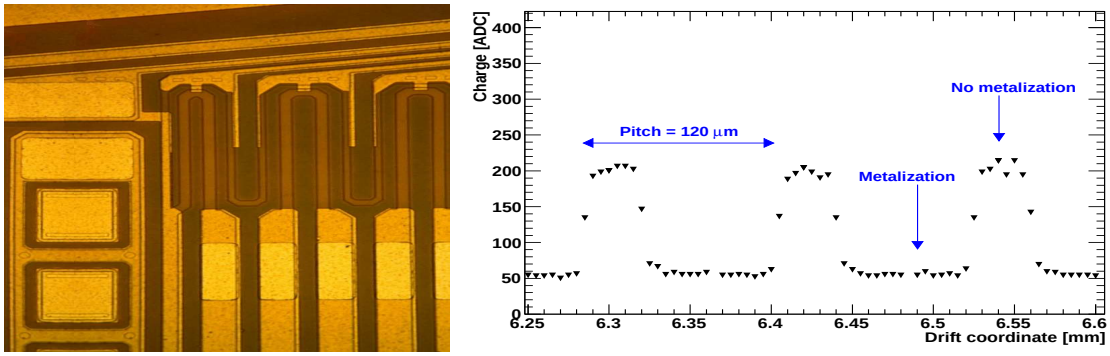

(a) (b)

Figure 3. (a) Picture of the SDD sensors (zoom): the cathode strips, the voltage divider (at the top) and the collection anodes (on the left) are visible. (b) The metal/oxide pattern of the SDD module visible from the laser signal peak vs drift coordinate.

2 Laser measurements

2.1 Fine position scanning

To check the dependence of the collected charge on the drift distance, a specific trajectory has been implemented in the motor controller, which moves the laser along the drift direction (i.e. perpendicular to the collection anode row) at a fixed anode coordinate.

The SDD module [7] has a row of 291 cathode strips perpendicular to the drift direction. A 85 μm wide metallization, which reflects the laser, covers the central part of each cathode (figure 3(a)). In order to properly generate a signal it is therefore necessary to center the laser spot on the 35 μm wide space between two Aluminum strips where no metal is present. A trajectory with a spatial gap of 5 μm between two consecutive laser shots has been implemented, to allow to select those in which the laser photons have not been reflected by the metallization. In figure 3(b) the value of charge peak (i.e. the ADC counts in the anode/time bin cell with highest signal) as a function of the laser position along the drift direction is plotted. It is possible to distinguish the metal/oxide pattern (pitch = 120 μm) of the SDD sensor: the flat regions in which the signal peak is low (50 ADC counts, close to the baseline value) correspond to the metallization while in the inter-cathode regions a peak signal of $\approx$ 200 ADC counts is observed.

The positions corresponding to the center of the *plateau* between two consecutive metallizations have been selected for the following analysis, in order to minimize possible biases due to laser reflection effects. In figure 4(a), the charge peak values are plotted as a function of the drift distance, corresponding to the known laser positions during the scanning. A decrease of the charge peak value with increasing drift distance is observed. It is due to the diffusion of the electron cloud during the drift, which causes a decrease of the peak together with an increase of the signal RMS. This is confirmed by figure 4(b), where the RMS values extracted from a Gaussian fit to the charge signals along time bins are plotted as a function of the drift distance.

In figure 5 the total collected charge calculated with the two-rectangle method described in section 1.2 and normalized to the maximum value is plotted as a function of the drift distance (cor-

2010 JINST 5 P02008

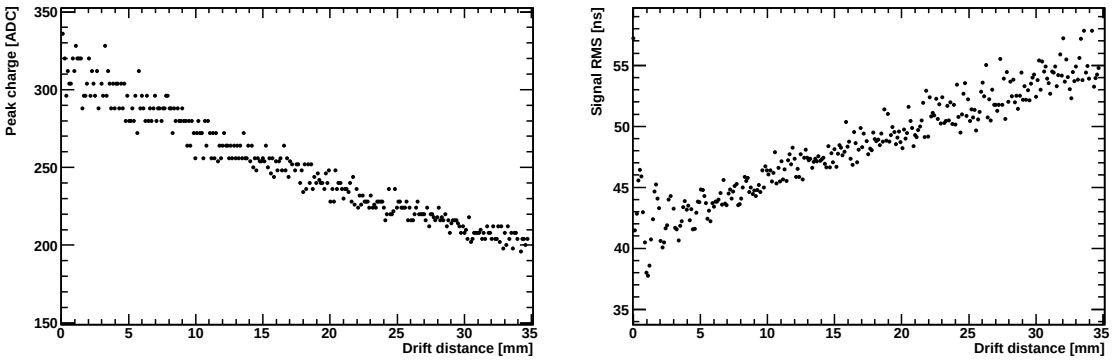

(a) (b)

Figure 4. Fine position scanning performed with $V_{gap} = 8$ V. (a) Charge peak values vs drift distance. (b) RMS along time-bins extracted from Gaussian fit to the charge signal vs drift distance.

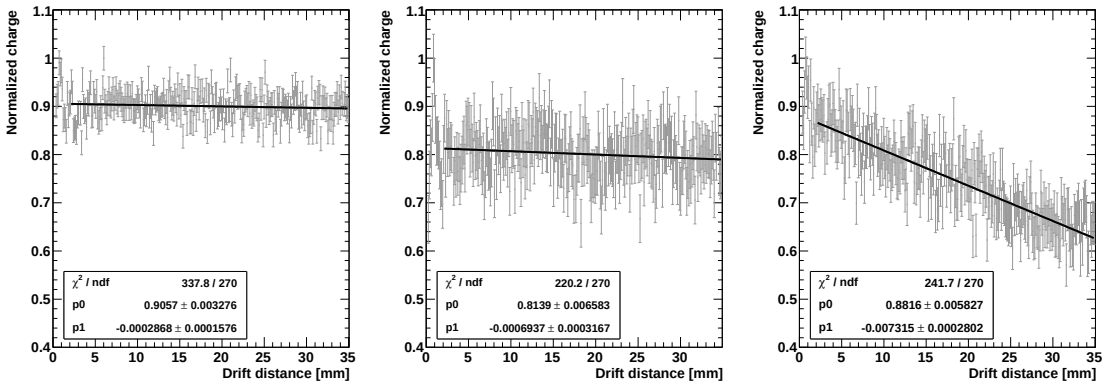

(a) (b) (c)

Figure 5. Collected charge vs laser drift position for three modules A, B and C.

responding to the known laser position) for the three modules. The error bars have been calculated from the RMS of the distribution of the counts summed over the *baseline rectangle*. Data have been fitted to a straight line of equation $c(x) = a + bx$. The first 2 mm ($\approx$ 10 time bins) of drift distance have not been taken into account for the fit, because it has been observed that at low time bins a strong effect of common mode noise (i.e. coherent fluctuations of all electronic channels) appears. It is probably induced by the laser generation when the trigger signal is issued by the motor control.

For the module A, displayed in figure 5(a), the collected charge is independent of the drift distance. The *p1* parameter of the linear fit is compatible with zero within 2σ and the maximum charge difference, calculated as the line slope multiplied by the maximum drift length (35.085 mm), is about 1%. In figure 5(b) (module B) the point-to-point charge fluctuations are larger than in the previous plot, because the module is affected by higher noise. The maximum charge difference is about 2%. The data for these two modules can also be fitted to a constant with a good χ^2 test

2010 JINST 5 P02008

Table 1. Voltage configurations used for the systematic study.

HV [V]	MV [V]	V_{gap} [V]	E_{drift} [V/cm]
-2368	-40	8	667
-2082	-45	7	583
-1791	-45	6	500
-1645	-45	5.5	458

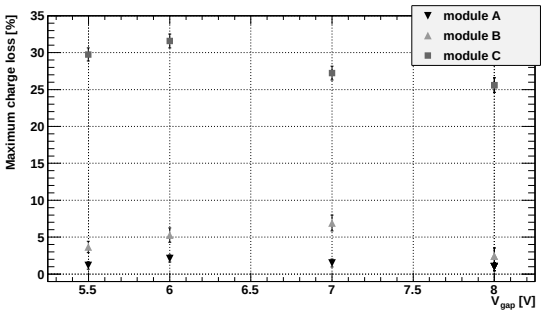

Figure 6. Maximum charge difference values vs voltage configuration.

value. In figure 5(c) (module C) a charge dependence on the drift distance is observable, with a maximum charge difference of about 26%. Module C, as mentioned in section 1.2, is affected by large inhomogeneities in the Silicon dopant distribution.

The same procedure was repeated for different voltage configurations, in order to search for possible dependence on the electrical drift field values. The chosen configurations are summarized in table 1. The nominal configuration used by the SDD modules mounted in the ALICE ITS is $V_{gap} = 6.04\,V$. This value has been chosen as a compromise between the highest signal peak over noise which is obtained at $V_{gap} = 8\,V$ and the better spatial resolution at lower V_{gap} provided by the larger cluster size due to diffusion effects.

In figure 6 the maximum charge differences for all the three modules as a function of V_{gap} are plotted. The charge difference values for module A are compatible with zero, allowing to conclude that no dependence of collected charge on drift time is present for all the applied E_{drift}. For module B a maximum charge difference of $\approx$5% for all voltage configuration is observed. In this case, the CCE seems to be independent of V_{gap}. Module C data present a decrease from 29% to 26% with increasing V_{gap}. For this particular module, a significant charge loss during the drift is observed and this loss is larger at lower values of drift speed, which correspond to larger drift times.

2.2 Fixed position

A second method for measuring the CCE has been developed in order to limit the systematic effects due to possible misalignments between the sensor plane and the laser support structure that can affect the scanning method described in the previous section. It consists in collecting different samples of 1500 laser shots in a fixed position with different values of V_{gap}, i.e. different values of the drift field. Since the drift time depends on the drift field as $t_d = x_d/(\mu_e E_d)$, the measurement at different V_{gap} allows to study the dependence of the collected charge on the drift time without mov-

2010 JINST 5 P02008

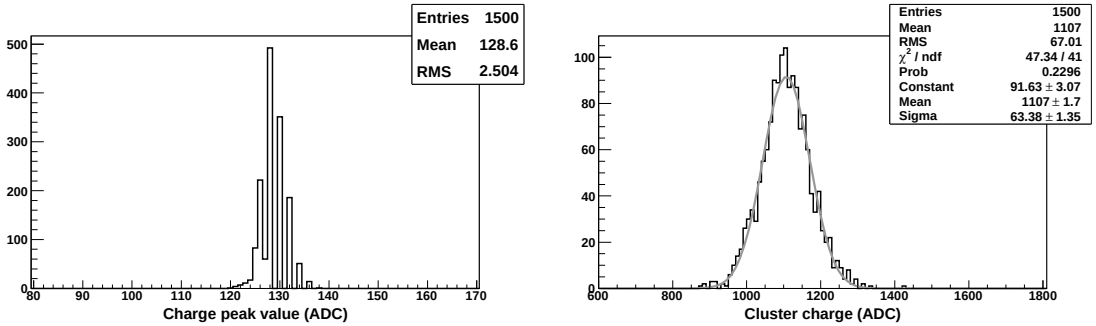

(a) (b)

Figure 7. Distribution of peak charge value (a) and total cluster charge (b) for 1500 events with $V_{gap} = 7$ V.

ing the laser spot on the detector surface. In order to limit systematic effects due to a drift in the laser intensity with time, or to possible displacements of the sensor caused by mechanical vibrations, the measurements were performed with a trigger rate of 100 Hz, thus limiting to 15 seconds the time for each sample at a fixed V_{gap}. For each position up to six values of V_{gap} in the range between 5.5 and 8 V were scanned, corresponding to a total measurement time for a given position of about 3 minutes, including the time to set up the system in between two measurements and the data acquisition system starting and stopping times. Moreover, the V_{gap} values were scanned in randomized order, thus canceling correlations between the drift field value and the time of the measurement.

For each event, the peak value (i.e. the ADC counts over the baseline in the anode/time bin cell with maximum charge), the position and the RMS of the laser signal along time bins and the total charge were extracted. The total charge has been obtained by subtracting the counts in the *baseline rectangle* from the counts in the *signal rectangle*, as explained in section 1.2.

In figure 7(a) the distribution of the charge peak values for 1500 events collected at $V_{gap} = 7$ V is shown. The effect of the lossy compression from 10 to 8 bit applied in AMBRA is visible: above 128 counts the Less Significant Bit (LSB) is dropped and the precision of the ADC counts is limited to 2 units. In figure 7(b) the distribution of the total collected charge is shown together with the result of a fit to a Gaussian function.

The drift time averaged over the 1500 events is reported in figure 8(a) as a function of the applied V_{gap} for a given fixed position of the laser shot. As expected, a linear decrease of drift time with increasing drift field is observed. In figure 8(b) the average value of peak charge as a function of the applied V_{gap} is shown: the value of peak charge increases when the drift field increases, as expected due to the smaller diffusion of the electron cloud during the shorter drift time. This is confirmed by the decrease of the RMS of the signal peak along the drift direction with increasing V_{gap}, as it can be seen in figure 8(c).

The values of the total charge averaged over the 1500 events are plotted as a function of V_{gap} in figure 9 for the modules A (left panel) and C (right panel) used in this study. In order to allow comparison of charge collected on different modules with different laser intensities, the total charge has been normalized to the value (in ADC counts) measured at $V_{gap} = 8$ V. The systematic error (gray band around the point) was estimated from the spread of the values of average cluster charge obtained repeating 6 times the measurement at a fixed position and at same V_{gap}. A clear

2010 JINST 5 P02008

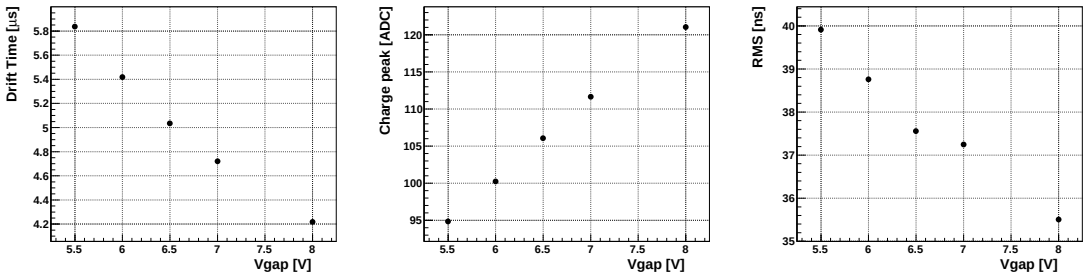

(a) (b) (c)

Figure 8. Drift time (a), charge peak (b) and RMS along drift direction (c) vs V_{gap}.

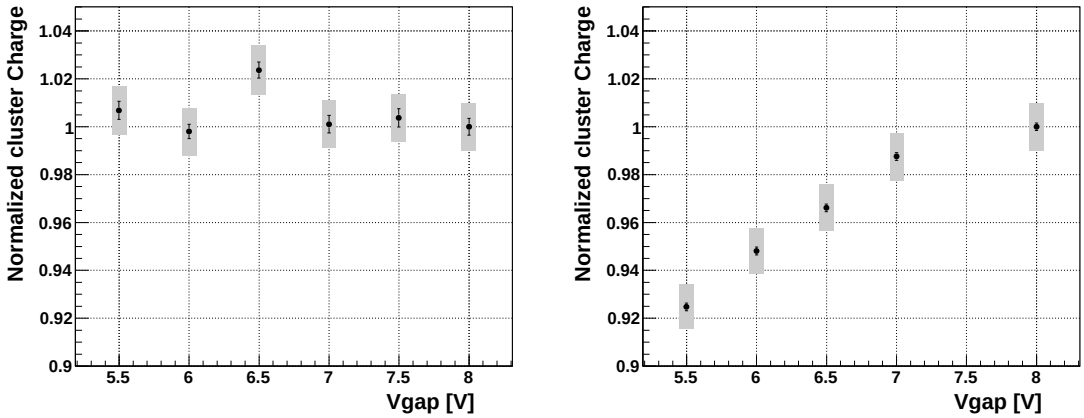

Figure 9. Total collected charge versus V_{gap} for module A (left) and module C (right).

dependence of the collected charge on the applied V_{gap} (i.e. on drift time) is observed for module C, while for module A the total charge is independent of the drift field, thus confirming the results obtained with the scanning technique described in the previous section.

The measurement has been performed shooting the laser in five different positions on the detector surface. For module A, all the measurements showed no dependence of the collected charge on the applied V_{gap}. For module C, in all the tested positions, it has been observed that the charge collected at the minimum drift field ($V_{\text{gap}} = 5.5$ V) is about 90% of the value measured at the maximum V_{gap} of 8 V.

3 Cosmic rays

A third method to study the CCE has been implemented. It is based on the measurement of the charge released by atmospheric muons in the SDD sensor. Using this method, which exploits the signal from charged (ionizing) particles, it is possible to avoid the possible systematic effects due to the laser reflection on the metallizations and to the common mode noise coming from the laser generation triggered by the motor controller.

2010 JINST 5 P02008

3.1 Trigger system for atmospheric muons

To study the collected charge at different drift positions in a SDD module with minimum ionizing particles, a dedicated trigger system detecting atmospheric muons has been built and operated. The system is composed of three plastic scintillators, a NIM crate for electronic devices and an acquisition system. Two of the scintillators are NE102A type with an area of 80 x 80 cm^2 and a thickness of 4 cm. The two scintillators are located one meter above and one meter below the SDD module respectively. Both of them cover the entire area of the module, but for technical reasons the centers were not aligned to the center of the module. The third is a 1 cm tick scintillator with an area of 7.5 x 7.5 cm^2. It is located above the SDD module, at 3 cm from the sensor surface. Due to mechanical constraints, it is not perfectly aligned to the SDD module and it does not cover its entire surface.

Each scintillator is shielded and equipped with a photo-tube that sends an analog signal to the electronic system. The analog signal is first discriminated and then sent to a coincidence unit for trigger purpose. The calibration of each scintillator is performed triggering with the two large scintillators, sending the analog signal of the scintillator to an ADC and looking at the single particle spectrum in ADC channel units. The discriminator threshold has been set to 20 mV for all the three signals and the voltage of the three photo-tubes has been set to ≈1700 V. A coincidence among these three scintillators in a time window of 100 ns gives the trigger signal to the SDD acquisition system.

With this trigger, atmospheric muons with direction between 0^o and 30^o with respect to the vertical direction are selected, providing an average trigger rate of about 0.2 Hz. Due to the geometrical arrangement of the system and some selection cuts on the cluster reconstruction in the SDD, 50% of the triggers select a muon crossing the SDD module that can be analyzed.

3.2 Results

Using the trigger system described in the previous paragraph, we collected about 40k cosmic events on SDD modules A and C, polarized with $V_{gap} = 8$ V. In order to study the effect of the zero-suppression, for module A, which did not show charge loss effects in the laser-based studies, a sample of muons was collected with the zero suppression active. In figure 10 the results for module A are shown (zero suppressed data). In the left panel, a profile of the peak charge values shows the decrease of peack charge with increasing of the drift time. The maximum decrease is about 47%. In the right panel it is possible to observe that the cluster size increases at larger drift times (profile plot). This behavior is consistent with the results obtained using the laser methods (see figures 4 and 8).

To study the dependence of the collected charge on the drift time, data have been acquired without zero suppression and, for each event, the charge of the cluster has been calculated with the method described in section 1.2.

Data have been divided in nine bins along the drift direction. For each bin the distribution of the collected charge has been fitted with a convolution of a Landau and a Gaussian. As an example, three of these distributions, one for a bin close to the anodes, one for the central region and one for a time interval far from the anodes (i.e. close to the center of the detector) are shown in figure 11.

2010 JINST 5 P02008

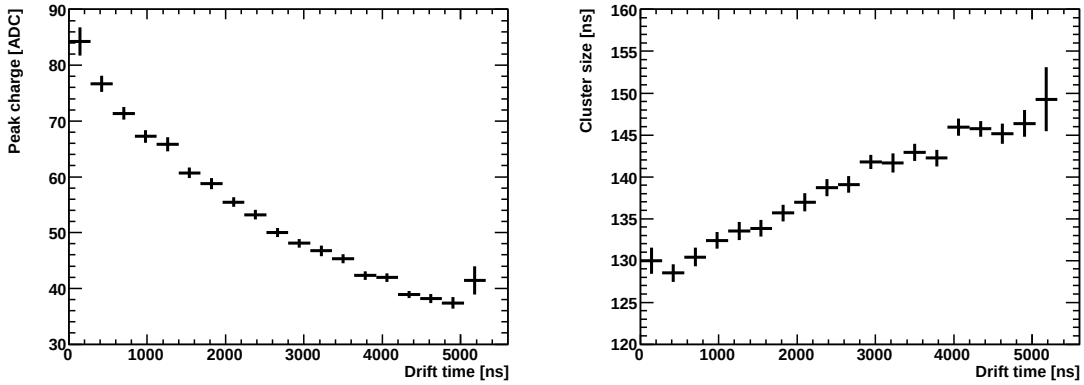

Figure 10. Cosmic-ray data collected with $V_{gap} = 8$ V. (a) Charge peak values vs drift time. (b) Cluster size values vs drift time.

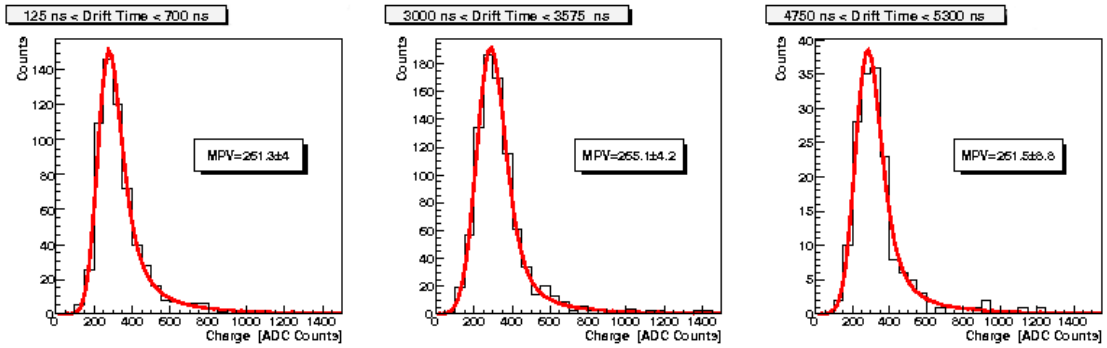

Figure 11. Distributions of collected charge in different drift time intervals, fitted to a convolution of a Landau and a Gaussian (without zero suppression).

The Most Probable Value (MPV) of the fit functions is then used in the study of charge dependence on drift time. In figure 12(a) the MPVs as a function of the drift time, for module A, are plotted for two sets of data (with and without zero-suppression). The triangular markers represent data acquired without zero-suppression in the CARLOS chip and they do not show a dependence of the collected charge on drift time. They can be fitted to a constant function. The circular markers represent data collected with zero-suppression and have been fitted to a straight line. In figure 12(b), the MPVs as a function fo the drift time obtained by a Monte Carlo simulation, including a detailed description of the detector and front-end response, are shown and fitted to a straight line. In case of zero-suppressed data, the difference between charge collected for muons crossing close to the anodes and muons with maximum drift distance amounts to ≈15% in case of data and to ≈17% in case of simulation. This confirms that the simulation correctly reproduces the detector response and the combined effect of charge diffusion and zero suppression on the collected charge, allowing to use a correction factor extracted by the Monte Carlo simulation in the offline data reconstruction.

In figure 13, the MPVs extracted from non-zero-suppressed events are plotted as a function of the drift time, for modules A and C. Data are normalized to the value at the lowest drift time. For module A (left panel), data are fitted to a constant. As seen in the previous plot, no decrease of the

2010 JINST 5 P02008

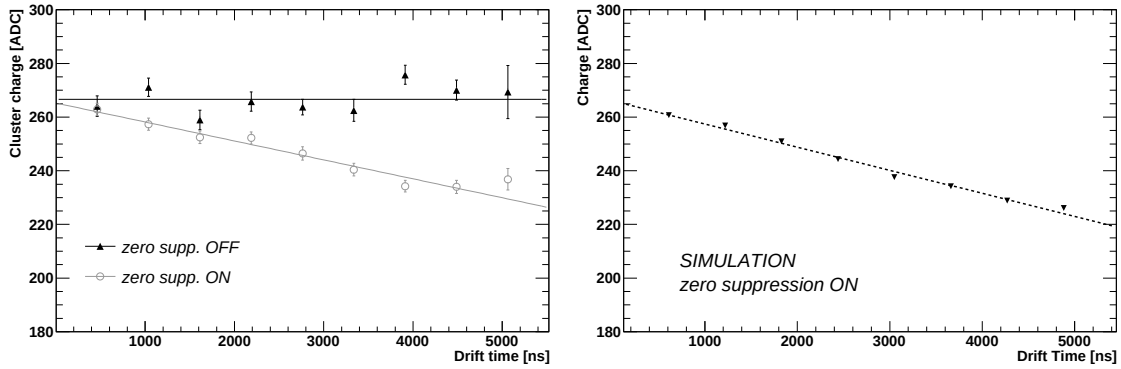

(a) (b)

Figure 12. (a) module A: MPVs versus drift time. Data taken without zero-suppression are fitted to a constant, data taken with zero-suppression on are fitted to a straight line. (b) Monte Carlo simulation: cosmic data taken with zero-suppression.

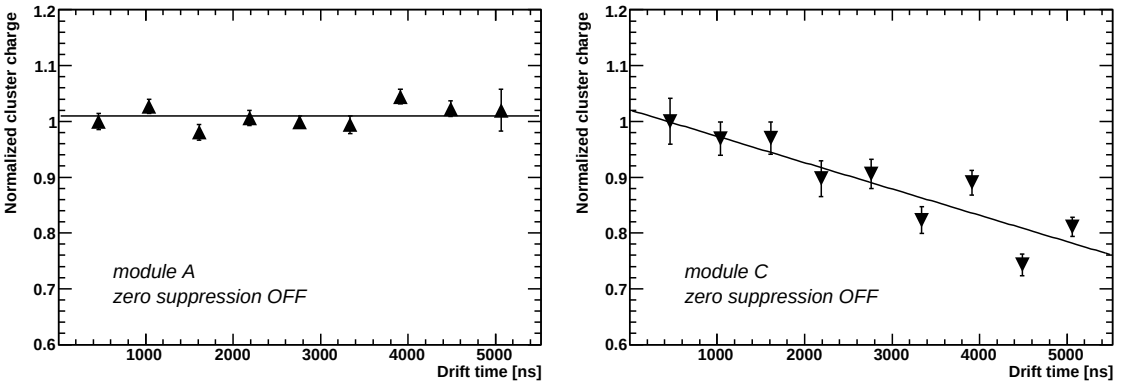

(a) (b)

Figure 13. MPVs versus drift time (normalized values). (a) Module A, data fitted to a constant. (b) Module C, data fitted to a straight line.

most probable value of the collected charge is present as a function of the drift time. On the contrary, for module C (right panel), a cluster charge dependence on the drift time is visible. Data have been fitted to a straight line. The maximum charge loss value, extracted from the fit, is ≈26%. This result is compatible with to the one obtained with the scanning methods using the infrared laser.

4 Conclusions

A systematic investigation of charge collection in the Silicon Drift Detectors has been performed on three sensors spared during the ALICE Inner Tracking System construction. The CCE has been investigated by studying the total cluster charge as a function of drift time/distance for signal events produced with an infrared laser and for atmospheric muon clusters. On modules with uniform dopant concentration (A and B), no dependence of the collected charge on the drift time

2010 JINST 5 P02008

has been observed, allowing to conclude that effects of electron trapping during the drift are negligible. On the contrary, on modules with large dopant inhomogeneities a significant decrease of collected charge with increasing drift time is observed, reaching a $\approx$ 26% difference between clusters produced close to the anodes and clusters produced in the center of the detector. It should be pointed out that for this kind of sensors (C), an inefficiency in charge collection was already measured during beam tests [13] and the significant inhomogeneities in dopant concentration were observed when mapping the detector response with the laser [6]. As a matter of fact, only 2 modules of the 260 that have been mounted on the ALICE Inner Tracking System have been built on the particular wafer type (C) and are expected to be affected by sizable systematic effects on charge collection efficiency.

It has also been shown that the zero-suppression algorithm applied to reduce the data size affects the measured cluster charge in a way that depends on the drift time: for larger drift times, the electron diffusion gives rise to wider cluster tails that are more likely to be cut by the thresholds applied when suppressing the zeroes. It should be pointed out that this effect can be accounted for when correcting the reconstructed cluster charge because it is quantitatively reproduced by detailed Monte Carlo simulation of the SDD detector response. This correction is possible because, also at large drift times, the peak charge values are higher than $\approx$20 times the average noise, as is it shown in figure 10.

Acknowledgments

We wish to thank the people helping us in setting up the mechanics and electronics of the SDD test station: F. Borotto, F. Cotorobai, M. Mignone and F. Rotondo. We wish to thank also the people involved in the assembly and bonding of the SDD modules, whose work was fundamental for the SDD project: F. Dumitrache, B. Pini and the teams from SRTIIE, Kharkov, the Ukraine. This work was partly supported by the European Union, the *Regione Autonoma Valle d'Aosta* and the *Ministero del Lavoro e della Previdenza Sociale*.

References

[1] E. Gatti and P. Rehak, *Semiconductor drift chamber. An application of a novel charge transport scheme*, *Nucl. Instrum. Meth.* **A 225** (1984) 608.

[2] S. Beolé et al., *Silicon drift detector. Studies about geometry of electrodes and production technology*, *Nucl. Instrum. Meth.* **A 377** (1996) 393.

[3] S. Beolé et al., *New developments in silicon drift detectors*, *Nuovo Cim.* **A 109** (1996) 1261.

[4] ALICE collaboration, B. Alessandro et al. *ALICE: Physics Performance Report, Volume II*, *J. Phys.* **G 32** (2006) 1295.

[5] ALICE collaboration, K. Aamodt et al., *The ALICE experiment at the CERN LHC*, 2008 *JINST* **3** S08002.

[6] G. Batigne et al., *Characterization of the ALICE Silicon Drift Detectors using an infrared laser*, 2008 *JINST* **3** P06004.

[7] ALICE collaboration, A. Rashevsky et al., *Characteristics of the ALICE silicon drift detector*, *Nucl. Instrum. Meth.* **A 461** (2001) 133.

2010 JINST 5 P02008

[8] ALICE collaboration, A. Rivetti et al., *The front-end system of the silicon drift detectors of ALICE*, *Nucl. Instrum. Meth.* **A 541** (2005) 267.

[9] G. Mazza, P. De Remigis and K. Kloukinas, *AMBRA: a multi-event buffering and readout ASIC for the silicon drift detectors of the ALICE experiment*, *IEEE Trans. Nucl. Sci.* **55** (2008) 2414.

[10] S. Antinori, D. Falchieri, A. Gabrielli and E. Gandolfi, *A rad-hard 2D-compreSSOR ASIC for ALICE SDD experiment*, *Nucl. Instrum. Meth.* **A 524** (2004) 295.

[11] S. Antinori et al., *Design and Test of the ALICE SDD Data Concentrator Card CARLOSrx*, *IEEE Nucl. Sci. Symp. Med. Imag.* (2006) 316.

[12] ALICE collaboration, A. Werbrouck et al., *Image compression for the silicon drift detectors in the ALICE experiment*, *Nucl. Instrum. Meth.* **A 471** (2000) 281.

[13] E. Crescio et al., *Results from beam tests of large area silicon drift detectors*, *Nucl. Instrum. Meth.* **A 539** (2005) 250.

2010 JINST 5 P02008